2D SnSe Nanonetworks; Growth and Evaluation for Li-ion Battery Applications

*Fionán Davitt[1], Killian Stokes[2], Timothy W. Collins[1], Manuel Roldan-Gutierrez[3], Fred Robinson[4], Hugh Geaney[2], Subhajit Biswas[*1], Shery L.Y. Chang[3], Kevin M Ryan[2], Gillian Reid[4] and Justin D. Holmes[1]*

[1]School of Chemistry & AMBER Centre, University College Cork, Cork, T12 YN60, Ireland. [2]Bernal Institute & Chemical Sciences Department, University of Limerick. [3]Eyring Materials Center and School of Molecular Sciences, Arizona State University, Tempe, AZ 85287, USA

[4]School of Chemistry, University of Southampton, Southampton SO17 1BJ, U.K.

*To whom correspondence should be addressed: Tel: +353 (0)21 4905143; E-mail: s.biswas@ucc.ie (SB)

Abstract

Engineered two-dimensional (2D) layered materials possess unique physical properties, with the potential to improve the performance and endurance of future electronic and energy devices. Here we report the growth of complex 2D nanonetworks of crystalline tin selenide (SnSe) via liquid injection chemical vapour deposition using a single source diselenoether precursor. Potential applications of SnSe span a wide range of technological areas, particularly in energy devices. The synthesized SnSe networks were composed of high surface area interconnected junctions of one dimensional (1D) nanowires in a 2D plane; such complex SnSe nanonetwork structures have not previously been reported. The SnSe networks possessed an orthorhombic Pnma 62 crystal structure throughout, with the individual network branches uniformly orientated along the <011> and <01-1> directions. The width of the individual interconnected nanowire branches ranged from 120 – 250 nm, with lengths

ranging from 1 to 4 μm. The networks of 1D nanowires had a layer thickness of 88 ± 10 nm. A growth mechanism for the formation of these networks is proposed based on the minimisation of high surface energy planes. We also highlight the potential of SnSe nanonetworks as anode material for Li-ion batteries, with galvanostatic testing showing an initial discharge capacity in excess of 1000 mAh g^{-1}, with a 92 % capacity retention after 50 cycles at a specific current of 100 mA g^{-1}.

Keywords: Nanowire networks, 2D materials, Layered materials, Chemical vapor deposition, SnSe, Li-ion battery

Introduction

The increasing demand on the Earths' resources, and the surge in interest in green technology, is fuelling research into new materials and new morphological design for efficient energy generation and storage devices. Metal chalcogenide materials, typically in the form of varying stoichiometries of MX [M=Pb, Cd, Zn, Ag, Sb, Sn, etc.; X=S, Se, Te] have shown great prospects for energy device applications.[1] Materials such as PbTe and Bi_2Te_3 have historically been popular in the field of thermoelectric materials,[2] however, avoiding scarce and environmentally toxic materials such as Pb, Bi and Te, is of great importance for such applications if they are to be sustainable. Similarly for photovoltaic applications, materials such as Pb and Cd based chalcogenides have been widely studied[3]. In comparison to these, other chalcogenide materials, such as SnSe, a relatively Earth abundant and non-toxic material, is an attractive option for sustainable energy device applications.[1] Indeed, SnSe has shown great promise for thermoelectric devices[4–7] and for solar cells[8–10] and has been reported to have a record high thermoelectric ZT value of 2.6 along its crystal b-axis.[9] In addition to these promising energy harvesting capabilities, SnSe also has great promise for applications in Li-ion batteries.[12–15] Commercial Li-ion batteries typically use graphite as an anode; possessing a capacity of ~372 mAh g^{-1}.[14] SnSe, however, is a very attractive material for improvement of improvement of Li-

ion batteries due to the high theoretical capacity of $Li_{4.4}Sn$ of 994 mAh g^{-1}, which sparked initial interest into thin film SnSe as an anode material.[15] Early results, however, showed a reduced capacity for SnSe based anodes of 400 mAh g^{-1} after 40 cycles, with improvements made in recent studies to as high as 1003 mAh g^{-1}.[14] Therefore there is a strong motivation to study SnSe as a promising alternative to other scarce and toxic chalcogenide materials for energy applications.[1]

SnSe is a layered metal chalcogenide material, formed from tightly bound chemical bonds across the *b* and *c* crystal axes, and weak van der Waals bonds across the longer *a*-axis direction. This weakly bound *a*-axis direction contributes to SnSe forming readily in 2D plate structures,[16] due to the slower crystal growth rate along this direction, and easier cleavage along this plane[17]. SnSe has also been shown to form as 1D nanowire structures.[18,19] Engineering the morphology of nanomaterials, such as in a 2D sheet or 1D nanowire form, is an ideal way to tune their material properties, as well as the scalability for device implementation.[20]

The controlled growth and structural engineering of nanomaterials has the potential to offer an untold impact on technology. Engineering materials in a nanostructure form allows incredible potential for device scaling to smaller dimensions, as well as presenting unique electrical, optical and mechanical properties, distinct from the bulk material.[21–23] 2D materials in particular are being heavily pursued for battery applications, with the 2D form offering many advantages over the bulk structure.[20,21] Further engineering of the material structure can lead to even more exotic nanostructures,[24] such as complex branched nanonetworks. These nanonetworks are formed from large groups of intersecting nanowires with single crystalline junctions, and have been shown to exhibit novel electrical, chemical and mechanical properties compared to their bulk counterparts.[25–27] In particular, nanonetworks with high porosity are an ideal energy harvesting platform (e.g. thermoelectric, photovoltaic, etc.), as the thermal conductivity is drastically reduced in such structures due to a combination of the high porosity

with increased backscattering at the nodes and enhanced light absorption due to high surface area.[28] In addition, a seamless network made of nanowires is also an ideal material for energy storage applications; combining the improved cyclability associated with nanowire battery materials[29] with stronger mechanical strength, while also maintaining a large exposed surface area to enhance electrolyte infiltration.[26]

Complex branched nanostructures exist for many technologically-important materials, such as Si[30] and III-V materials like GaN[30], GaP[31] and GaSb.[32] Branched chalcogenide nanomaterials such as MoS_2[33] and CdTe[34] have been produced through solution methods, and branched PbS[35] and PbSe[36] nanostructures have been grown though various bottom-up CVD growth methods. SnSe has been shown to form in both 2D plate structures[16,37,38] and 1D nanowire structures[18,19] via chemical vapour deposition (CVD) methods, but engineering the nanowires in a seamless 2D network structure of SnSe has thus far proved elusive. The 2D nature of the layered SnSe material can act as a constraint in one direction to confine the network to a 2D plane. Further controlled reaction mechanics, such as energetically preferred crystal growth directions or selective surface passivation, then act to restrict the lateral growth into a nanowire-like form along the 2D plane, resulting in a 2D network of nanowires, which grow in the same x-y plane. $TiSi_2$, which crystallises in a similar layered structure to SnSe, has been shown to form in a branched 2D nanonetwork where the branched nanowires all lie within the same plane[39,40].

Herein we report for the first time the growth of single crystalline 2D networks of SnSe nanowires, forming large complex branched structures. These networks are grown through the use of an atmospheric pressure CVD method, using a single source [$SnCl_4${^{n}BuSe$(CH_2)_3$Se^{n}Bu}] precursor[41] without any growth catalysts. The growth of these networked SnSe nanowires instead relies on the nucleation of localised high surface energy sites, and the subsequent surface energy minimisation of

these sites, which leads to the growth of nanowire networks with low surface energy faceted planes. We report electrochemical data from these SnSe nanonetworks, presenting them as a promising material for future high performance Li-ion battery applications.

Results and Discussion

SnSe nanonetworks were synthesised (see Supporting Information for detailed experimental method) using a liquid-injection CVD method at 550 °C, injecting [$SnCl_4\{^nBuSe(CH_2)_3Se^nBu\}$] as a single source precursor[41] (precursor concentration of 7.5 mg ml^{-1}) at a constant rate of 1.5 ml h^{-1} under a constant flow of 1.1 SCCM of argon gas. The nanonetworks were grown on a Si substrate, which was placed at the centre of the furnace. The morphology, structural and chemical composition of the nanonetworks synthesised at 550 °C is shown in Figure 1. Figure 1(a) shows an SEM image of the networks, with an AFM topography image shown in Figure 1(b), highlighting large 2D plate-like structures, 30 – 40 μm in dimension and around 88 ± 10 nm thick (see supporting information figure S1 for additional AFM measurements and average thickness value), that are composed of many interconnected nanowire-like branches, approximately 120 nm wide. The lengths of the individual branches in the network vary from a few hundred nanometres to up to ~4 μm. This branched nature of the networks presents a greatly increased surface to volume area as compared to a uniform flake (supplementary information Figure S2). Figure 1(c) shows an XRD pattern taken from the network sample shown in Figure 1(a) and can be assigned to phase pure orthorhombic SnSe (Pnma 62 orthorhombic, JCPDS 48-1224). The most intense peak in the XRD pattern is seen to be the (400) peak, demonstrating significant ordering of the 2D nanonetworks on the Si substrate. The (400) plane corresponds to the plane along which SnSe layers are stacked, and the observation of a relatively strong (400) XRD peak is commonly seen for 2D SnSe[42]. Figure 1(d) shows a TEM image of a section of these network branches after removal from the growth substrate. The networks are 2D in nature and

are seen to lie flat on the TEM grid, with the nanowire branches all lying within the same plane, in a perpendicular manner to each other. The structural nature of these 2D nanonetworks closely resembles that of previously reported $TiSi_2$ nanonetworks[39,40]. The inset shows an EDX spectrum taken from the area highlighted in blue, showing an atomic percent ratio of 53:47 Sn:Se in the wire branches, presenting further evidence for the formation of stoichiometric SnSe. Raman analysis on these nanonetworks is shown in Figure 1(e), and exhibits the B_g vibrational mode of SnSe at ~107 cm^{-1}, and also the modes corresponding to the SnSe A^2_g and A^3_g modes at 129 cm^{-1} and 151 cm^{-1}, respectively[43]. These values are in agreement with previously reported values for ultrathin SnSe flakes[44].

The detailed crystal structure of the individual branches was analysed using high resolution TEM (HRTEM), as shown in Figure 1(f). The HRTEM image was taken from a junction area of the network, and this particular junction is highlighted in red in the low resolution TEM image of the nanonetwork structure shown in Figure 1(d). The bottom right inset of Figure 1(f) shows a magnified HRTEM image of an area of the branch, with a measured d-spacing of 0.299 nm which corresponds to the (011) and (0-11) lattice planes of Pnma 62 orthorhombic SnSe (JCPDS 48-1224). The top right inset shows a selected area electron diffraction (SAED) pattern taken from the area highlighted in purple in Figure 1(d). Diffraction spots in this SAED are assigned to Pnma 62 orthorhombic SnSe (JCPDS 48-1224) viewed down the [100] zone axis. The individual nanowire branches of these networks are seen to exhibit a growth direction in either the <011> or <0-11> directions (Figure 1(f)). The angles between the (011) and (0-11) diffraction spots were found to be ~93°, with the angle between the (011) and (01-1) spots being ~87°. These are low surface energy planes for orthorhombic SnSe[47,48], making these network structures energetically favourable due to the maximum exposure of these low energy surface planes. Previous reports on single SnSe nanowires have shown that these planes are also prevalent growth directions for simple 1D SnSe geometries[18]. The (001) and (010) planes are however expected to be higher surface energy planes and should exhibit an initially higher growth rate. From the TEM

image of Figure 1(d), it is apparent that the network branches are not fully uniform in roughness along their length, and many expanded sites on the edges of the branches are seen in the low resolution TEM image (green circle in Figure 1(d)). These irregularly expanded surface regions are proposed to be initiated from growth along the (001) and (010) planes. These surface edge sites are thought to act as nucleation sites for further branching. If the reaction was allowed to continue, it is proposed that these (001) and (010) planes would then be subsequently supressed by lower surface energy planes, leading to further branch formation along the (011) and (01-1) planes. This will be discussed in detail while discussing the growth mechanism of the nanonetworks.

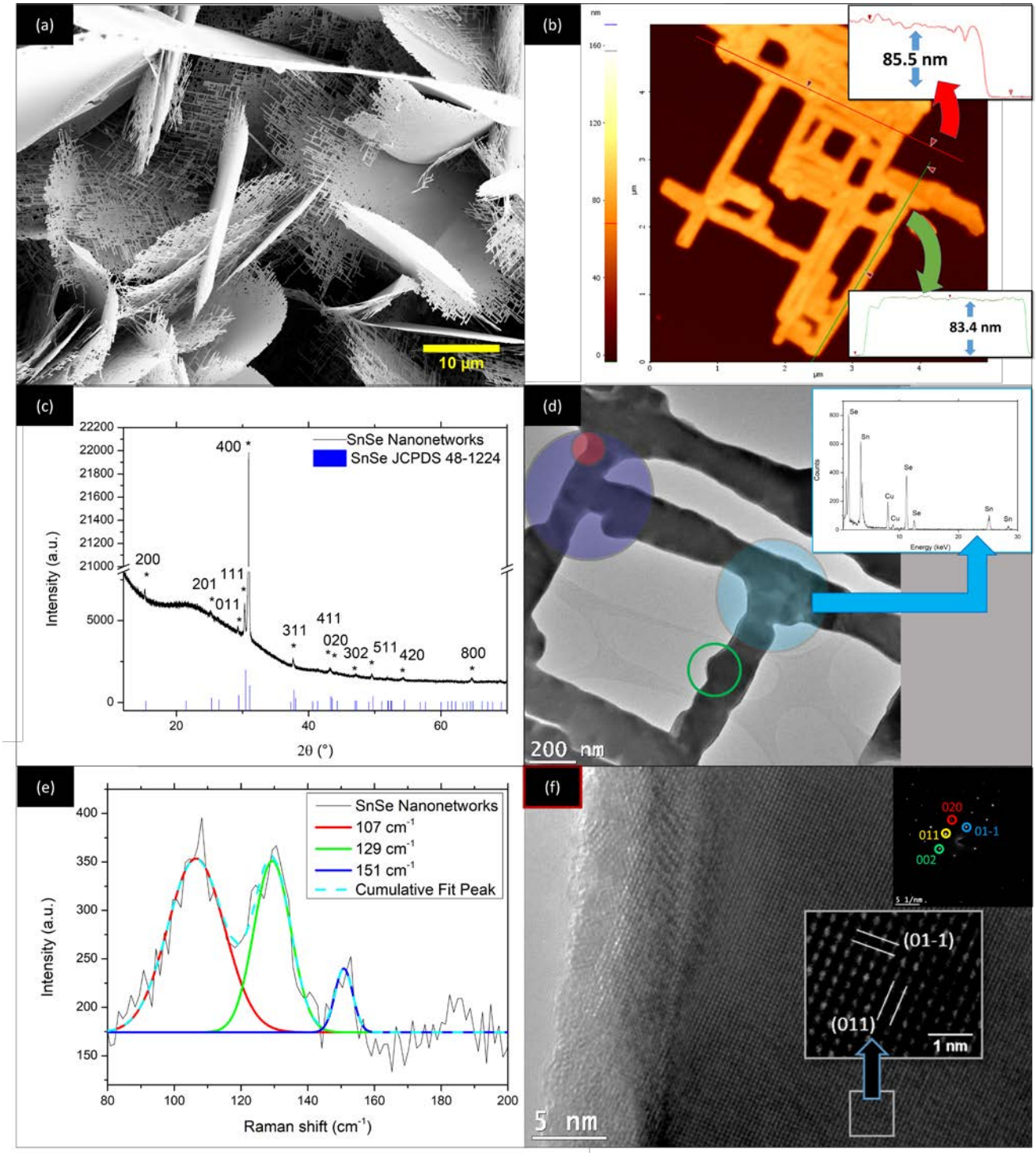

Figure 1: Analysis of the structure and composition of the nanonetworks. (a) SEM image of the SnSe nanonetworks, showing a large amount of interconnected nanowires growing from 2D plate structures. (b) AFM analysis of the SnSe nanonetworks, after dropcasting onto a Si wafer. Thickness profiles are shown in the two insets. (c) XRD analysis of the sample shown in **(a)**, indexed to Pnma 62 orthorhombic SnSe (JCPDS 48-1224). The broad peak in the region of ~22° is due to the glass slide

upon which the sample was placed for the XRD measurement. (d) Low magnification TEM image of a section of a SnSe nanonetwork. The inset shows an EDX spectrum of the area highlighted in blue, showing an atomic percent ratio of Sn:Se of 53:47. Raman analysis was performed on the SnSe nanonetworks, as shown in Figure 1(e). The peaks seen correspond to the B_g vibrational mode of SnSe at ~107 cm^{-1}, and the SnSe A^2_g and A^3_g modes at 129 cm^{-1} and 151 cm^{-1}, respectively.[43] (f) HRTEM image of the area highlighted in (d) in red, showing the high-quality single crystal structure of the SnSe networks. The measured lattice spacing confirms that the growth direction of the branches are along the <011> and <0-11> directions. This area is also at the interface of two meeting branches, and importantly shows no significant crystal defects at this intersection. The inset shows an SAED pattern of the area highlighted in purple in (d), showing a crystal structure indexed to Pnma 62 orthorhombic SnSe (JCPDS 48-1224). This also indicates that the growth direction of the branches is along the <011> and <0-11> directions.

The participation of a surface energy minimisation mechanism in the growth of the SnSe networks was further investigated through detailed TEM analysis. Figure 2(a) shows a low magnification TEM image of a SnSe nanonetwork. The network shows a highly uniform nature, with the angles between all the interconnected nanowires in the network visually appearing to form in a perpendicular manner to each other. From the SAED pattern shown in Figure 1(d) it is expected that these branches should be formed along the <011> and <0-11> directions, which for a Pnma SnSe crystal (JCPDS 48-1224) makes an angle of 93.822 ° between the (011) and (0-11) planes and 86.178 ° between the (011) and (01-1) planes. Measuring the angles between the branches in Figure 2(a) reveals angles of 93° and 87° between the wires in the nanonetwork, in close agreement with the calculated values. This provides further evidence for the uniform growth of the branches along these particular directions. Outside of these regular branches marked in red, a small amount of additional growth is also seen, particularly between the junctions of two meeting branches (Figure 2(a)). The intersection of multiple branches is

highlighted in the different coloured boxes with corresponding arrows. Figure 2(b) shows a schematic of the SnSe crystal structure in the proposed network form, viewed down the [100] direction. The branches are assigned to the <011> equivalent directions. Additional growth along the <010> and <001> directions at the branch intersections, as shown in the schematic of Figure 2(b), results in a simulated structure strongly resembling the TEM image of Figure 2(a), indicating that additional growth has occurred along these directions. The intersecting nanonetwork junction highlighted by the purple circle in Figure 2(a) is shown in detail in Figure 2(c), with a webbed structure seen between the two branches (white box). This webbed structure indicates growth along the <001> direction. Figure 2(d) shows a lattice resolved HAADF STEM image of a junction region, revealing a highly ordered single crystalline structure. This clearly shows the branches as <011> and <01-1> growth, with the additional inter-junction growth along the <001> direction. The thin amorphous layer seen at the surface of the network is composed of SnO_x (see EELS and EDX map in the Supporting Information of Figures S3, S4 and S5) , which is expected to have formed after exposure to atmospheric conditions, on removal from the CVD chamber, as seen before for previous reports on SnSe.[47]

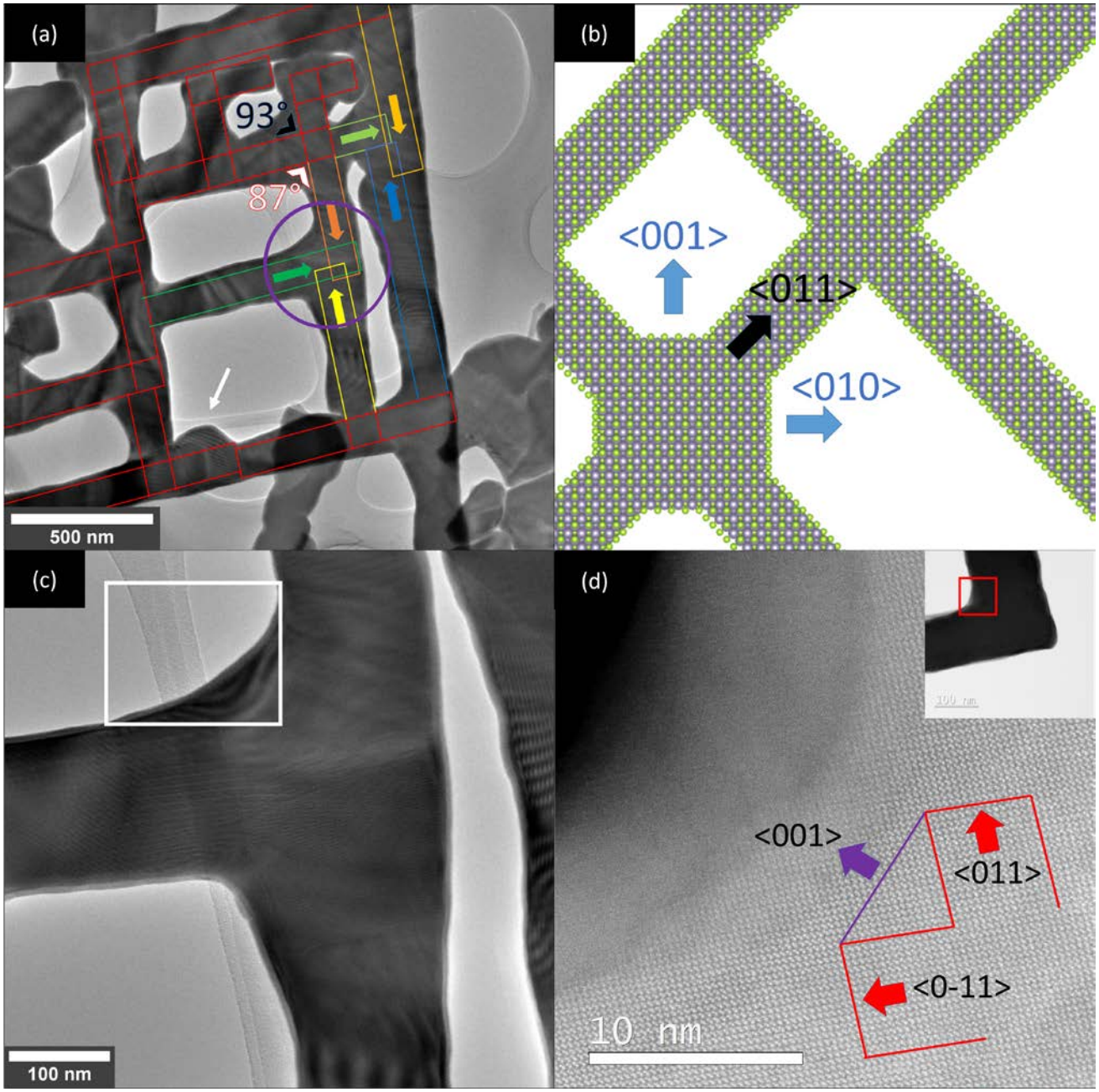

Figure 2: Analysis of the structure of the individual nanowire branches in a network: (a) Low magnification TEM image of a section of a nanonetwork. All of the branches are seen to form in a regular manner to each other, at angles of 93° and 87° to each branch. (b) Illustration of the predicted SnSe structure, based on the crystal data inferred from Figure 1, showing the growth direction of the branches along the <011> and <0-11> directions. (c) TEM image of the SnSe network junction within the purple circle in **(a)**. (d) High resolution STEM image of a single crystalline junction, with the branches assigned as growth in the <011> and <0-11> directions. Additional growth along the <001>

direction at the junction interface is observed. Inset shows the junction region that the high resolution image is taken from.

A growth model; borrowing knowledge from the TEM and HRTEM observations; explaining the growth of SnSe nanonetworks is proposed in Figure 3. The (010) and (001) planes have previously been calculated to be high energy surface planes for an orthorhombic SnSe structure,[46] which should exhibit a initially high growth rate. The growth rate of these planes is expected to decrease as the reaction progresses, as the crystal system tries to minimise its surface energy by forming lower energy surface planes. Based on this, the growth is predicted to start with the nucleation of small (010) and (001) faceted SnSe flakes, as shown in Figure 3(a). As the growth continues, surface energy minimisation results in the appearance of the lower surface energy (011) and (0-11) planes as is shown in Figure 3(b), with these low surface energy planes eventually dominating the growth (Figure 3(c)). However, changes in the favoured growth planes could be induced through small changes in reaction equilibrium, such as temperature or gas flow fluctuations (leading to precursor vapour pressure variations). Changes in such reaction conditions have previously been shown to alter the preferred growth planes in $TiSi_2$ nanonetworks[40]. These changes in reaction equilibrium could lead to the reappearance of a small number of (010) and (001) surface planes, as shown in Figure 3(d). Defects induced by the interaction between the meeting of two <011> nanowire branches could also lead to a change in locally favoured growth planes (additional <010> and <001> growth is seen at the meeting of three branches in Figure 2(c). These planes would then grow until the growth along these planes again became unfavourable, and the low-energy (011) and (01-1) plane growth would begin to dominate once again (Figure 3(e)). Maximisation of these low surface energy planes would then continue, with the growth progressing predominantly in the <011> and <01-1> directions, leading to a protruded edge site on the wire structure (Figure 3(e)). The white arrow in figure 2(a) indicates an example of this in the nanonetwork. This edge site would then act as a nucleation site for the branch

growth, with continuation of growth along the <011> and <01-1> directions then leading to the network structure as shown in Figure 3(f). Notably the webbed-like structure between the junctions of the nanowire branches, which is seen in Figure 3(f), is also seen in the TEM image in Figure 2(c) (white box).

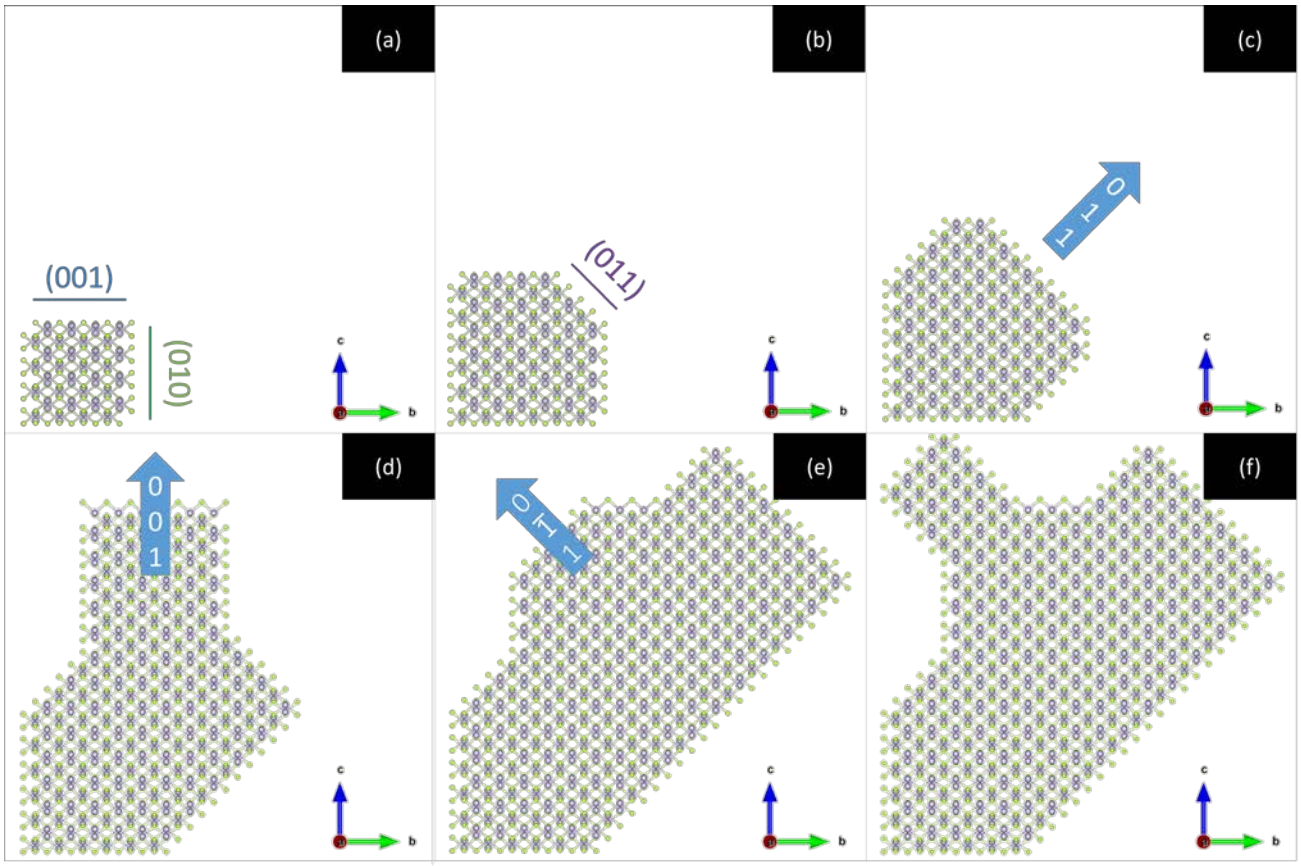

Figure 3: Proposed growth mechanism of the SnSe nanonetworks. (a) Initial {010} and {001} faceted SnSe flake is formed. (b) From this initial nucleation site, the flake continues to grow, with the gradual appearance of the lower surface energy {011} planes. (c) As the growth progresses, the high surface energy {010} and {001} planes are replaced with the lower surface energy {011} and {0-11} planes. (d) Small disturbances in the reaction equilibrium as the growth progresses results in the sporadic reappearance of a small number of {010} and {001} planes. (e) Surface energy minimisation results in the repression of these high surface energy planes with {011} equivalent planes, leading to these

{010} and {001} planes acting as nucleation sites for additional <011> directed branches. (f) The growth continues along these <011> planes, leading to the networked SnSe structure.

Many factors can contribute to the nucleation and growth rate of crystal facets in CVD reactions, such as growth temperature, precursor concentration, chamber pressure, etc. In an attempt to further control the growth of these SnSe nanonetworks, the reaction was performed at a higher temperature (Figure 4) and then also at varying initial precursor concentrations (Figure 5). SEM images in Figure 4 show the comparison in network morphology for the growth at 550 and 600 ºC. A higher growth temperature is expected to yield a greater preference for high energy surface planes.[50] This is seen by increased growth of the less stable (001) and (010) planes, leading to increased density in branching with the branches that form being highly uneven along their length (see Figure 4, which shows the networks formed as a function of temperature). This increased density in branching resulted in a less porous 2D network nanostructure at 600 ºC compared to the growth at 550 ºC (Figure 4).

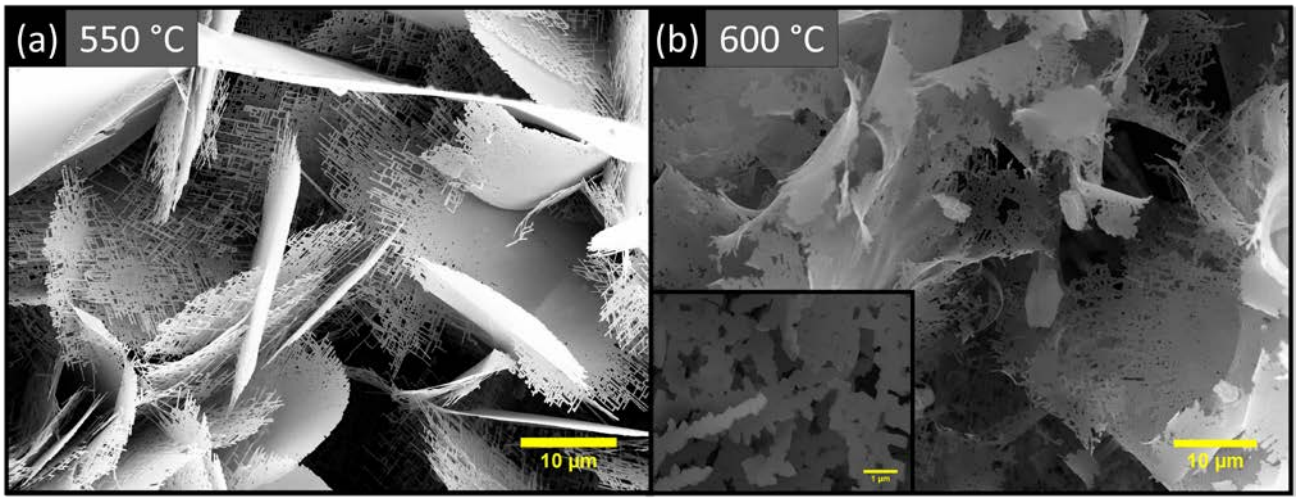

Figure 4: Growth of the SnSe structures as a function of growth temperature. (a) was performed at a furnace temperature of 550 °C and (b) at 600 °C.

Preforming the growth at a fixed temperature (550 ºC), whilst varying the initial precursor concentration (3.75 mg/ml, 7.5 mg/ml and 15 mg/ml), was also examined to observe the effect of limiting and increasing the precursor vapour influx to the crystal surface. However, this was seen to have very little influence on the structure of the final product in terms of dimension and branching density (Figure 5).

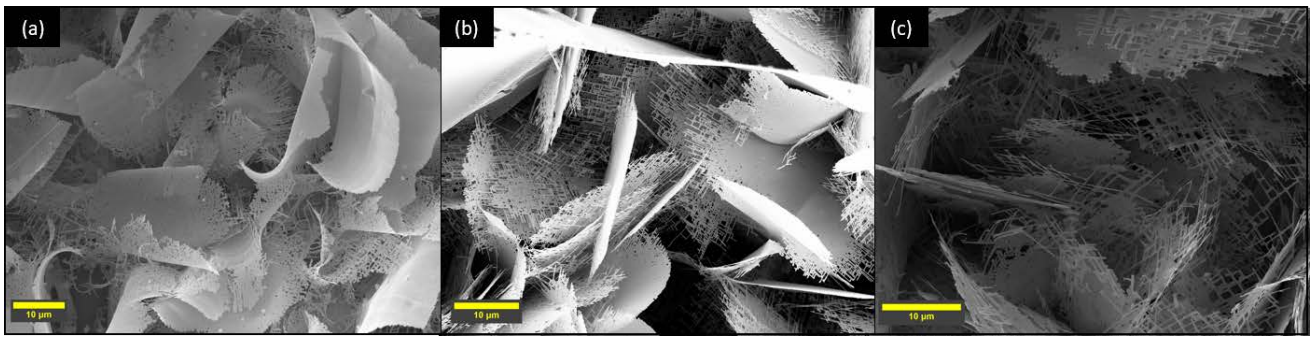

Figure 5: Growth of the SnSe structures as a function of initial precursor concentration at 550 ºC. Part (a), (b) and (c) shows growth with 3.75 mg/ml, 7.5 mg/ml and 15 mg/ml respectively.

Galvanostatic testing was carried out to assess the use of the SnSe nanonetworks as a potential anode material for Li-ion battery applications. To facilitate these tests, SnSe nanonetworks were grown directly on stainless steel current collectors. For electrochemical testing, SnSe nanonetworks were achieved at a growth temperature of 550 °C with 7.5 mg/ml precursor concentration. This growth condition was selected for electrochemical testing as previous growth at 550 °C produced a network structure with highest porosity and uniformity (Figure 4), whereas changing precursor concertation had minimal effect on the network morphology (Figure 5). Small changes in the morphology of the 2D network structures were observed in the networks grown on stainless steel compared to that grown on silicon substrate, such as branch width and length, etc. (Figure 5b and Supporting Information Figure S6). The initial discharge capacity was in excess of 1000 mAh g^{-1} and showed a 92 % capacity retention after 50 cycles at a specific current of 100 mA g^{-1} (Figure 6(a)), which compares favourably with previously reported SnSe anodes (Supporting Information, Table S1 shows comparison with published

SnSe electrochemical data). This capacity retention is drastically improved compared to other pure (i.e. not formed from a nanocomposite material) SnSe morphologies, where capacity retention is typically <35 % at this point[10,14]. Reduction of the volume of battery anode materials through nanostructuring has been shown to have a positive impact on the capacity retention of the device[29], and we ascribe this improvement of the SnSe nanonetworks compared to non-structured SnSe to the better ability of the networks to accommodate the volume changes typically associated with Li insertion and removal. The voltage profiles shown in Figure 6(b) are consistent with the occurrence of conversion reactions at higher potentials (i.e. between ~1 V and 3 V) and Li alloying below ~1 V.

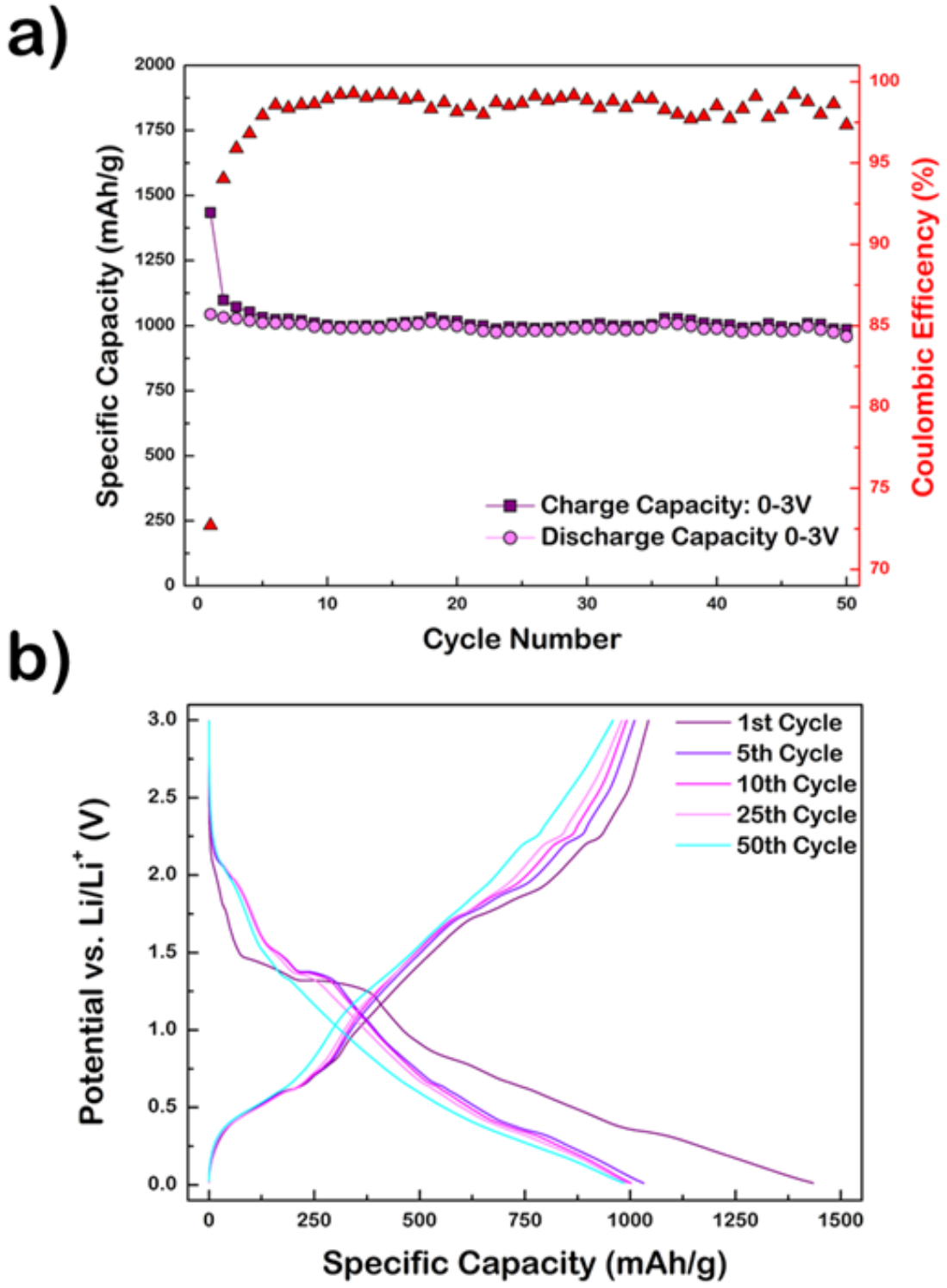

Figure 6: a) Capacity retention summary for the SnSe nanonetworks tested at a specific current of 100 mA/g and b) corresponding voltage profiles for the 1st, 5th, 10th, 25th and 50th cycle.

Examination of the differential capacity plots, shown in Figure 7, shows clear peaks that match extremely well with the peak locations presented by Lee *et al.*[10] during their combination of ex-situ XRD and DQ/DV analysis. The peak locations from the DQ/DV analysis are consistent with the transformation of the SnSe nano-networks to Sn and Li_2Se during the lithiation down to ~1 V, followed by lithiation of the Sn via an alloying process. The reverse processes are identified for delithiation, with the persistent peaks above 1 V for the 50 cycles, suggesting excellent reversibility for Se related conversion reactions.

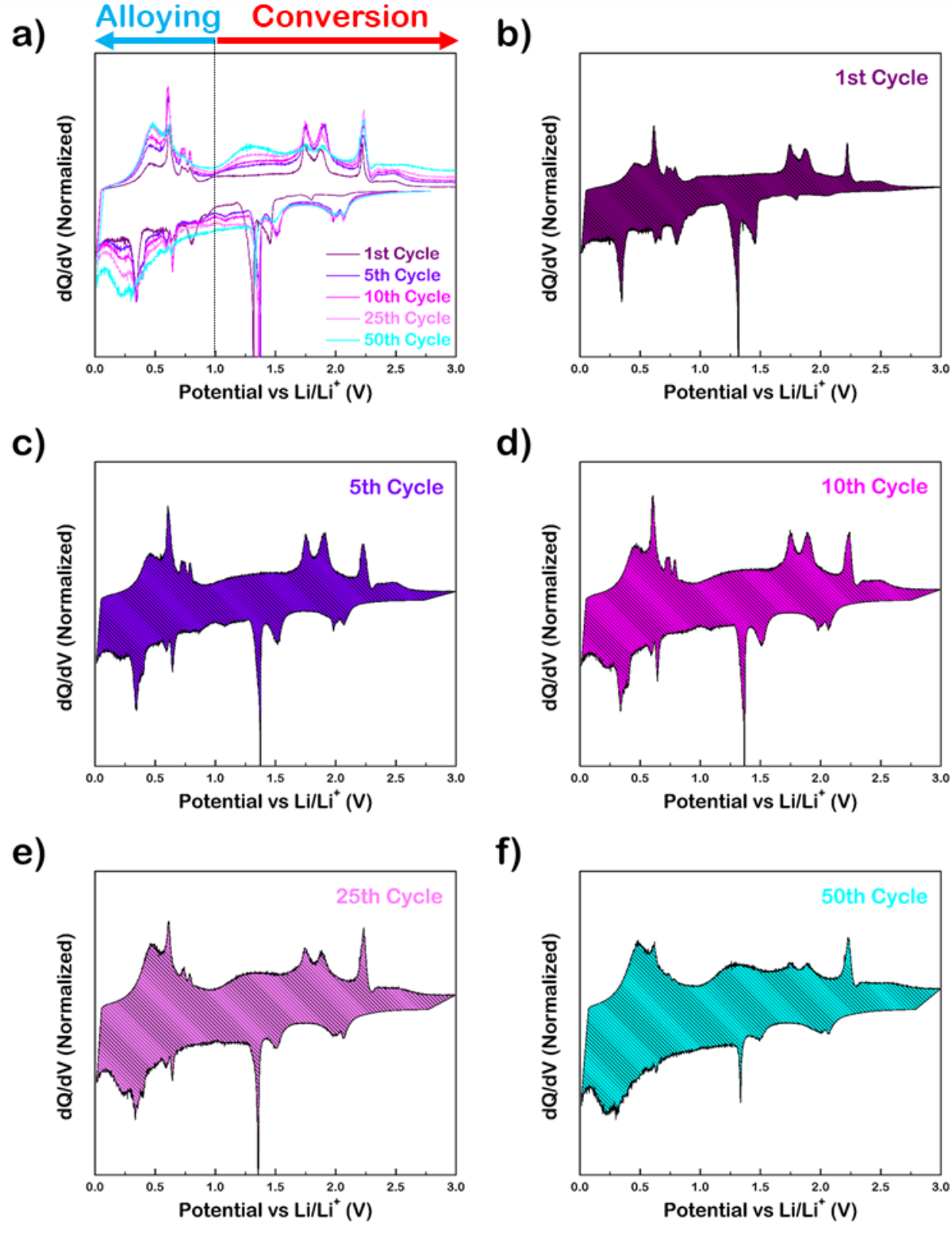

Figure 7: a) Combined differential capacity plot for the 1st, 5th, 10th, 25th and 50th cycle for the galvanostatic test shown in Figure 6. Individual plots of the differential capacity for the 1st (b), 5th (c), 10th (d), 25th (e) and 50th (f) cycle.

Conclusions

Previously unexplored complex 2D SnSe nanonetwork structures have been grown via an atmospheric pressure CVD method, utilising a single source [$SnCl_4\{^nBuSe(CH_2)_3Se^nBu\}$] precursor, without the presence of an external catalysing agent. These 2D networks were seen to consist of many interconnected nanowires, with a nanowire width of about ~120 nm and thickness of ~88 nm. The lengths of these wires within the network were between 100 nm and 4 μm long. These nanowires were seen to join at regular uniform junctions at an angle of either 87° or 93° to one another, attributed to every wire having either a <011> or <0-11> growth direction throughout the network. Minimisation of the surface energy of the crystal planes was proposed to be the driving force behind the formation of these porous network structures, consistent with the prevalence of the (011) and (0-11) SnSe planes in the final structure. Owing to the porosity induced by the internal nanowire substructure that is present in complex 2D SnSe nanonetworks such as these, a correspondingly higher surface area to volume ratio is justified compared to an equivalent uniform 2D SnSe flake. These SnSe nanonetworks show great promise for for Li-ion battery devices, exhibiting a high initial discharge capacity, in excess of 1000 mAh g^{-1}, and maintaining a 92 % capacity retention after 50 cycles at a specific current of 100 mA g^{-1}. These values show a significant enhancement compared to previously reported values for pure SnSe nanocrystals, and this is attributed to the combination of the SnSe network morphology and the correspondingly higher surface area. Further control in the nucleation of the branch sites through future experimental design changes (high vacuum set-ups, etc.), could lead to even greater manipulation of the porosity of the network, and hence further potential control of the surface area and the material properties. The results demonstrated here on the growth of SnSe nanonetworks and their energy storage device application, presents motivation for the continued research into the electrochemical potential of this material system. For example, a future study could aim at complete electrochemical analysis of the SnSe network nanomaterial within different voltage windows *e.g.* isolating alloying, conversion, and finding a ‘sweet spot’ between the two to obtain the optimal cycling parameters for

the SnSe network electrodes. This research also instigates future potential for engineered hierarchical networked structures (e.g. 2D network with different porosity, branching orientation, thickness, diameter or even 3D network structure) of energy relevant materials for energy storage (Li-ion battery) and energy harvesting (thermoelectric, photovoltaic, etc.) applications.

Supporting Information:

Experimental method, a table detailing the performance of SnSe anodes in the literature, AFM analysis of the SnSe nanonetworks, surface area to volume ratio of a networked structure, EELS and EDX analysis, SEM image of the SnSe nanonetworks grown on stainless steel.

Conflict of Interest:

The authors declare no competing financial interest.

Acknowledgements:

This research was funded by Science Foundation Ireland (Grants: 12/RC/2278 and 14/IA/2513). KR acknowledges Science Foundation Ireland grants 16/IA/4629 and 16/ M-ERA/3419. K.S. acknowledges the Irish Research Council for funding through the Government of Ireland Postgraduate Scheme. H.G. acknowledges the SIRG under grant no. 18/SIRG/5484 and Enterprise Ireland under contract no. CF20144014. G.R. acknowledges EPSRC and Deregallera for a studentship to F.R. (EP/N509747/1). The facilities and staff at the Advanced Microscopy Laboratory at Trinity College Dublin are acknowledged for their support.

References:

(1) Gao, M. R.; Xu, Y. F.; Jiang, J.; Yu, S. H. Nanostructured Metal Chalcogenides: Synthesis, Modification, and Applications in Energy Conversion and Storage Devices. *Chem. Soc. Rev.* **2013**, *42*, 2986–3017.

(2) Twaha, S.; Zhu, J.; Yan, Y.; Li, B. A Comprehensive Review of Thermoelectric Technology: Materials, Applications, Modelling and Performance Improvement. *Renew. Sustain. Energy Rev.* **2016**, *65*, 698–726.

(3) Zhang, G.; Finefrock, S.; Liang, D.; Yadav, G. G.; Yang, H.; Fang, H.; Wu, Y. Semiconductor Nanostructure-Based Photovoltaic Solar Cells. *Nanoscale* **2011**, *3*, 2430–2443.

(4) Hernandez, J. A.; Ruiz, A.; Fonseca, L. F.; Pettes, M. T.; Jose-Yacaman, M.; Benitez, A. Thermoelectric Properties of SnSe Nanowires with Different Diameters. *Sci. Rep.* **2018**, *8*, 1–8.

(5) Chen, Z. G.; Shi, X.; Zhao, L. D.; Zou, J. High-Performance SnSe Thermoelectric Materials: Progress and Future Challenge. *Prog. Mater. Sci.* **2018**, *97*, 283–346.

(6) Chandra, S.; Banik, A.; Biswas, K. N -Type Ultrathin Few-Layer Nanosheets of Bi-Doped SnSe: Synthesis and Thermoelectric Properties. *ACS Energy Lett.* **2018**, *3*, 1153–1158.

(7) Chandra, S.; Biswas, K. Realization of High Thermoelectric Figure of Merit in Solution Synthesized 2D SnSe Nanoplates via Ge Alloying. *J. Am. Chem. Soc.* **2019**, *141*, 6141–6145.

(8) Franzman, M. A.; Schlenker, C. W.; Thompson, M. E.; Brutchey, R. L. Solution-Phase Synthesis of SnSe Nanocrystals for Use in Solar Cells. *J. Am. Chem. Soc.* **2010**, *132*, 4060–4061.

(9) Liu, S.; Guo, X.; Li, M.; Zhang, W. H.; Liu, X.; Li, C. Solution-Phase Synthesis and Characterization of Single-Crystalline SnSe Nanowires. *Angew. Chemie - Int. Ed.* **2011**, *50*, 12050–12053.

(10) Minnam Reddy, V. R.; Gedi, S.; Pejjai, B.; Park, C. Perspectives on SnSe-Based Thin Film Solar Cells: A Comprehensive Review. *J. Mater. Sci. Mater. Electron.* **2016**, *27*, 5491–5508.

(11) Zhao, L.-D.; Lo, S.-H.; Zhang, Y.; Sun, H.; Tan, G.; Uher, C.; Wolverton, C.; Dravid, V. P.;

Kanatzidis, M. G. Ultralow Thermal Conductivity and High Thermoelectric Figure of Merit in SnSe Crystals. *Nature* **2014**, *508*, 373–377.

(12) Lee, D.-H.; Park, C.-M. Tin Selenides with Layered Crystal Structures for Li-Ion Batteries: Interesting Phase Change Mechanisms and Outstanding Electrochemical Behaviors. *ACS Appl. Mater. Interfaces* **2017**, *9*, 15439–15448.

(13) Zhang, Z.; Zhao, X.; Li, J. SnSe/Carbon Nanocomposite Synthesized by High Energy Ball Milling as an Anode Material for Sodium-Ion and Lithium-Ion Batteries. *Electrochim. Acta* **2015**, *176*, 1296–1301.

(14) Im, H. S.; Lim, Y. R.; Cho, Y. J.; Park, J.; Cha, E. H.; Kang, H. S. Germanium and Tin Selenide Nanocrystals for High-Capacity Lithium Ion Batteries: Comparative Phase Conversion of Germanium and Tin. *J. Phys. Chem. C* **2014**, *118*, 21884–21888.

(15) Wang, W.; Li, P.; Zheng, H.; Liu, Q.; Lv, F.; Wu, J.; Wang, H.; Guo, S. Ultrathin Layered SnSe Nanoplates for Low Voltage, High-Rate, and Long-Life Alkali–Ion Batteries. *Small* **2017**, *13*, 1–7.

(16) Cheng, Y.; Huang, J.; Li, J.; Cao, L.; Xu, Z.; Luo, X.; Qi, H.; Guo, P. SnSe/r-GO Composite with Enhanced Pseudocapacitance as a High-Performance Anode for Li-Ion Batteries. *ACS Sustain. Chem. Eng.* **2019**, *7*, 8637–8646.

(17) Xue, M. Z.; Yao, J.; Cheng, S. C.; Fu, Z. W. Lithium Electrochemistry of a Novel SnSe Thin-Film Anode. *J. Electrochem. Soc.* **2006**, *153*, 270–274.

(18) Huang, Y.; Li, L.; Lin, Y. H.; Nan, C. W. Liquid Exfoliation Few-Layer SnSe Nanosheets with Tunable Band Gap. *J. Phys. Chem. C* **2017**, *121*, 17530–17537.

(19) Nicolosi, V.; Chhowalla, M.; Kanatzidis, M. G.; Strano, M. S.; Coleman, J. N. Liquid Exfoliation of Layered Materials. *Science (80-.).* **2013**, *340*, 1226419–1226419.

(20) Shi, L.; Zhao, T. Recent Advances in Inorganic 2D Materials and Their Applications in Lithium and Sodium Batteries. *J. Mater. Chem. A* **2017**, *5*, 3735–3758.

(21) Rojaee, R.; Shahbazian-Yassar, R. Two-Dimensional Materials to Address the Lithium Battery Challenges. *ACS Nano* **2020**, *14*, 2628–2658.

(22) Liu, J.; Jian, J.; Yu, Z.; Zhang, Z.; Cao, B.; Du, B. Catalyst-Free Vapor Phase Growth of Ultralong SnSe Single-Crystalline Nanowires. *Cryst. Growth Des.* **2017**, *17*, 6163–6168.

(23) Butt, F. K.; Mirza, M.; Cao, C.; Idrees, F.; Tahir, M.; Safdar, M.; Ali, Z.; Tanveer, M.; Aslam, I. Synthesis of Mid-Infrared SnSe Nanowires and Their Optoelectronic Properties. *CrystEngComm* **2014**, *16*, 3470.

(24) Hu, J.; Odom, T. W.; Lieber, C. M. Chemistry and Physics in One Dimension: Synthesis and Properties of Nanowires and Nanotubes. *Acc. Chem. Res.* **1999**, *32*, 435–445.

(25) Gao, H.; Ji, B.; Jäger, I. L.; Arzt, E.; Fratzl, P. Materials Become Insensitive to Flaws at Nanoscale: Lessons from Nature. *Proc. Natl. Acad. Sci. U. S. A.* **2003**, *100*, 5597–5600.

(26) Goldstein, A. N.; Echer, C. M.; Alivisatos, A. P. Melting in Semiconductor Nanocrystals. *Science (80-.).* **1992**, *256*, 1425–1427.

(27) Wang, J.; Duan, H. L.; Huang, Z. P.; Karihaloo, B. L. A Scaling Law for Properties of Nano-Structured Materials. *Proc. R. Soc. A Math. Phys. Eng. Sci.* **2006**, *462*, 1355–1363.

(28) Manna, L.; Milliron, D. J.; Meisel, A.; Scher, E. C.; Alivisatos, A. P. Controlled Growth of Tetrapod-Branched Inorganic Nanocrystals. *Nat. Mater.* **2003**, *2*, 382–385.

(29) Liu, X.; Lin, Y.; Zhou, S.; Sheehan, S.; Wang, D. Complex Nanostructures: Synthesis and Energetic Applications. *Energies* **2010**, *3*, 285–300.

(30) Cheng, C.; Fan, H. J. Branched Nanowires: Synthesis and Energy Applications. *Nano Today* **2012**, *7*, 327–343.

(31) Bierman, M. J.; Jin, S. Potential Applications of Hierarchical Branching Nanowires in Solar Energy Conversion. *Energy Environ. Sci.* **2009**, *2*, 1050–1059.

(32) Verdier, M.; Lacroix, D.; Termentzidis, K. Thermal Transport in Two- and Three-Dimensional Nanowire Networks. *Phys. Rev. B* **2018**, *94*, 1–7.

(33) Chan, C. K.; Peng, H.; Liu, G.; McIlwrath, K.; Zhang, X. F.; Huggins, R. A.; Cui, Y. High-Performance Lithium Battery Anodes Using Silicon Nanowires. *Nat. Nanotechnol.* **2008**, *3*, 31–35.

(34) Wang, D.; Qian, F.; Yang, C.; Zhong, Z.; Lieber, C. M. Rational Growth of Branched and Hyperbranched Nanowire Structures. *Nano Lett.* **2004**, *4*, 871–874.

(35) Dick, K. A.; Deppert, K.; Larsson, M. W.; Mårtensson, T.; Seifert, W.; Wallenberg, L. R.; Samuelson, L. Synthesis of Branched "nanotrees" by Controlled Seeding of Multiple Branching Events. *Nat. Mater.* **2004**, *3*, 380–384.

(36) Yan, C.; Li, X.; Zhou, K.; Pan, A.; Werner, P.; Mensah, S. L.; Vogel, A. T.; Schmidt, V. Heteroepitaxial Growth of GaSb Nanotrees with an Ultra-Low Reflectivity in a Broad Spectral Range. *Nano Lett.* **2012**, *12*, 1799–1805.

(37) Jia, Y.; Ma, Y.; Lin, Y.; Tang, J.; Shi, W. Facile Synthesis of Branched MoS 2 Nanowires. *Chem. Phys.* **2018**, *513*, 209–212.

(38) Kuno, M.; Ahmad, O.; Protasenko, V.; Bacinello, D.; Kosel, T. H. Solution-Based Straight and Branched CdTe Nanowires. *Chem. Mater.* **2006**, *18*, 5722–5732.

(39) Bierman, M. J.; Lau, Y. K. A.; Kvit, A. V.; Schmitt, A. L.; Jin, S. Dislocation-Driven Nanowire Growth and Eshelby Twist. *Science (80-.).* **2008**, *320*, 1060–1063.

(40) Zhu, J.; Peng, H.; Marshall, A. F.; Barnett, D. M.; Nix, W. D.; Cui, Y. Formation of Chiral Branched Nanowires by the Eshelby Twist. *Nat. Nanotechnol.* **2008**, *3*, 477–481.

(41) Boscher, N. D.; Carmalt, C. J.; Palgrave, R. G.; Parkin, I. P. Atmospheric Pressure Chemical Vapour Deposition of SnSe and SnSe2 Thin Films on Glass. *Thin Solid Films* **2008**, *516*, 4750–4757.

(42) Gurnani, C.; Hawken, S. L.; Hector, A. L.; Huang, R.; Jura, M.; Levason, W.; Perkins, J.; Reid, G.; Stenning, G. B. G. Tin(<scp>iv</Scp>) Chalcogenoether Complexes as Single Source Precursors for the Chemical Vapour Deposition of SnE $_2$ and SnE (E = S, Se) Thin Films. *Dalt.*

Trans. **2018**, *47*, 2628–2637.

(43) Zhou, S.; Liu, X.; Lin, Y.; Wang, D. Spontaneous Growth of Highly Conductive Two-Dimensional Single-Crystalline TiSi2nanonets. *Angew. Chemie - Int. Ed.* **2008**, *47*, 7681–7684.

(44) Zhou, S.; Liu, X.; Lin, Y.; Wang, D. Rational Synthesis and Structural Characterizations of Complex TiSi2 Nanostructures. *Chem. Mater.* **2009**, *21*, 1023–1027.

(45) De Groot, C. H.; Gurnani, C.; Hector, A. L.; Huang, R.; Jura, M.; Levason, W.; Reid, G. Highly Selective Chemical Vapor Deposition of Tin Diselenide Thin Films onto Patterned Substrates via Single Source Diselenoether Precursors. *Chem. Mater.* **2012**, *24*, 4442–4449.

(46) Vaughn, D. D.; In, S. Il; Schaak, R. E. A Precursor-Limited Nanoparticle Coalescence Pathway for Tuning the Thickness of Laterally-Uniform Colloidal Nanosheets: The Case of SnSe. *ACS Nano* **2011**, *5*, 8852–8860.

(47) Chandrasekhar, H. R.; Humphreys, R. G.; Zwick, U.; Cardona, M. Infrared and Raman Spectra of the IV-VI Compounds SnS and SnSe. *Phys. Rev. B* **1977**, *15*, 2177–2183.

(48) Luo, S.; Qi, X.; Yao, H.; Ren, X.; Chen, Q.; Zhong, J. Temperature-Dependent Raman Responses of the Vapor-Deposited Tin Selenide Ultrathin Flakes. *J. Phys. Chem. C* **2017**, *121*, 4674–4679.

(49) Han, G.; Popuri, S. R.; Greer, H. F.; Bos, J. W. G.; Zhou, W.; Knox, A. R.; Montecucco, A.; Siviter, J.; Man, E. A.; MacAuley, M.; Paul, D. J.; Li, W. G.; Paul, M. C.; Gao, M.; Sweet, T.; Freer, R.; Azough, F.; Baig, H.; Sellami, N.; Mallick, T. K.; Gregory, D. H. Facile Surfactant-Free Synthesis of p-Type Snse Nanoplates with Exceptional Thermoelectric Power Factors. *Angew. Chemie - Int. Ed.* **2016**, *55*, 6433–6437.

(50) Ma, X. H.; Cho, K. H.; Sung, Y. M. Growth Mechanism of Vertically Aligned SnSe Nanosheets via Physical Vapour Deposition. *CrystEngComm* **2014**, *16*, 5080–5086.

(51) Tian, H.; Wang, X. F.; Mohammad, M. A.; Gou, G. Y.; Wu, F.; Yang, Y.; Ren, T. L. A Hardware Markov Chain Algorithm Realized in a Single Device for Machine Learning. *Nat. Commun.*

2018, *9*, 1–11.

(52) Hu, Z.; Zheng, D.; Tu, R.; Yang, M.; Li, Q.; Han, M.; Zhang, S.; Zhang, L.; Goto, T. Structural Controlling of Highly-Oriented Polycrystal 3C-SiC Bulks via Halide CVD. *Materials (Basel).* **2019**, *12*, 1–10.